

Evaluation of multi-parameter likelihoods through iteration of two-dimensional slices

JOEL S. JAYSON¹¹Retired

ABSTRACT

In this paper we introduce a method for resolving multi-parameter likelihoods by fixing all parameter values, but two. Evaluation of those two variables is followed by iteratively cycling through each of the parameters in turn until convergence. We test the technique on the temperature power spectrum of the lensed cosmic microwave background (CMB). That demonstration is particularly effective since one of the six parameters that define the power spectra, the power spectrum amplitude, A_s , nears linearity at small deviations, reducing computation to incrementation in one-dimension, rather than over a 2D grid. At each iterative step A_s is paired with a different parameter. The iterative process yields parameter values in agreement with those derived by *Planck*, and results are obtained within a few hundred calls for spectra. We further compute parameter values as a function of maximum multipole, ℓ_{\max} , spanning a range from $\ell_{\max}=959$ to 2500, and uncover bi-modal behavior at the lower end of that range. In the general case, in which neither variable is linear, we identify moderating factors, such as changing both parameters each iterative step, reducing the number of steps per iteration. Markov chain Monte Carlo (MCMC) computation has been the dominant instrument for evaluating multi-parameter functions. For applications with a quasi-linear variable such as, A_s , the 2D iterative method is orders of magnitude more efficient than MCMC.

Keywords: Computational Methods—Cosmology—Cosmological Parameters

1. INTRODUCTION

We evaluate multi-parameter likelihoods by freezing all parameter values, with the exception of two. Upon solution of those two parameters we step to a second pair, continuing in this fashion through all parameters, and then repeating the process until convergence. The temperature power spectrum of the cosmic microwave background (CMB) provides a ready example for demonstration.

The study of CMB power spectra is a mature subject (G. Hinshaw et al. 2013; *Planck* Collaboration 2020b) and provides a solid basis for comparison. Further, of the six parameters needed to define a spectrum, one of them is the amplitude, A_s . With no lensing A_s is proportional to the power spectrum. We incorporate lensing in our analysis, which introduces nonlinearity. Nevertheless, if variations in amplitude are small, the assumption of linearity introduces little error. The presence of the quasi-linear parameter, A_s , affords an opportunity to appreciably reduce the number of calls for power spectra computation, incrementing in one dimension,

rather than over a two dimensional grid. We introduce an algorithm to take full advantage of that opportunity. In general we fix A_s at each computational step, and multiply the power spectrum by a factor, γ , which serves as the amplitude variable. In the iterative process A_s is updated at each succeeding step with the algorithm,

$$A_{s,k+1} = \gamma_k A_{s,k}, \quad (1)$$

where k is the parameter step number. As the iterative process proceeds, γ approaches unity, and the introduced error approaches zero.

The evaluation of the Hubble parameter, H_0 , is in an ambiguous state, with differing estimations between low red shift measurements (W. L. Freedman et al. 2019; A. G. Riess et al. 2022), and CMB measurements (G. Hinshaw et al. 2013; *Planck* Collaboration 2020b), but also with some variation within each of those subsets. We focus on the CMB measurements herein. The two primary satellite CMB measurements were conducted by the *Planck* Collaboration, and before that the Wilkinson Microwave Anisotropy Probe (*WMAP*). *Planck* Collaboration (2020b) derive a value of $H_0=67.4\pm0.5 \text{ km s}^{-1} \text{ Mpc}^{-1}$ with a maximum mul-

tipole, $\ell_{\max}=2508$. G. E. Addison et al. (2016), using *Planck* data with $\ell_{\max}=1000$, exact a value of $69.7 \pm 1.7 \text{ km s}^{-1} \text{ Mpc}^{-1}$, a discrepancy that is slightly more than 1σ . The *WMAP* result with $\ell_{\max}=1200$, is $H_0=70.0 \pm 2.2 \text{ km s}^{-1} \text{ Mpc}^{-1}$ (G. Hinshaw et al. 2013).

The Atacama Cosmology Telescope (ACT) Collaboration (S. K. Choi et al. 2020; S. Aiola et al. 2020) derived a value of $H_0=67.9 \pm 1.5 \text{ km s}^{-1} \text{ Mpc}^{-1}$ within the multipole range of $\ell=575\text{--}4325$, and extracted a value of $67.6 \pm 1.1 \text{ km s}^{-1} \text{ Mpc}^{-1}$ when combining the *ACT* data with that of *WMAP* to provide coverage of the lower part of the multipole range. *ACT* is one of two earth bound telescopes observing CMB. The South Pole Telescope (*SPT*) is the second one. They report a value of $H_0=68.3 \pm 1.5 \text{ km s}^{-1} \text{ Mpc}^{-1}$ (L. Balkenhol et al. 2023). When combining the *SPT* data with that of *Planck* they find, $H_0=67.24 \pm 0.54 \text{ km s}^{-1} \text{ Mpc}^{-1}$, and when combining the *SPT* data with that of *WMAP* a value of $H_0=68.2 \pm 1.1 \text{ km s}^{-1} \text{ Mpc}^{-1}$. In summary, the CMB H_0 means fall in either the range $\sim 67.4\text{--}68.3$, or $\sim 69.7\text{--}70.0 \text{ km s}^{-1} \text{ Mpc}^{-1}$, the latter range found at $\ell_{\max} \leq 1200$. A review of H_0 evaluations can be found at L. Verde et al. (2024). Using our iterative procedure, we evaluate the CMB parameters as a function of ℓ_{\max} , with the aim of shedding light on H_0 variations within CMB evaluations..

Section 2 introduces the ln likelihood function and its partial derivatives. We provide an example, which employs two variables, γ , and H_0 , to illustrate the solution of the two partial derivatives..

Section 3 addresses the iterative solutions. In Section 3.1 the quasi-linear approach, using A_s in all iterative steps, is employed to derive the CMB parameters for the *Planck* data with $\ell_{\max}=2500$. Four runs were conducted, each with a different set of initial values, all producing similar results with small variance, and in agreement with *Planck* results (*Planck* Collaboration 2020b) that were obtained using the Markov chain Monte Carlo (MCMC) method (N. Metropolis, et al. 1953; W. K. Hastings 1970). The maximum number of calls for power spectra computations for any of the runs is less than 600. In Section 3.2 the quasi-linear analysis is applied to evaluate CMB parameters as a function of ℓ_{\max} . We find bi-modal behavior for the *Planck* results for $\ell_{\max} \leq 1259$, and an explanation for the variant H_0 CMB values. In Section 3.3 the general case, no quasi-linear parameter, is briefly discussed. In applications where a parameter equivalent to A_s is lacking, calls for computing the associated function are incremented over a two dimensional grid. We identify factors that work towards reducing the number of power spectra calls in that instance. In Section 4 we discuss the results, and present our conclusions.

2. 2D MAXIMUM LIKELIHOOD ESTIMATE

The *Planck* Collaboration advanced the most accurate and precise CMB results to date (*Planck* Collaboration

2020b), and we use their data in this study. Though *Planck* observations covered the entire sky, the data used to compute the CMB power spectra excludes the Galactic plane, and was processed by the *Planck* Collaboration to provide a full sky equivalent. At high multipoles the likelihood distribution for a full sky tends to a Gaussian (W. J. Percival & M. L. Brown 2006). The *Planck* data and the computed power spectra are binned as described in *Planck* 2018 results V (*Planck* Collaboration 2020a). We select a bin size of $\Delta\ell=30$ spanning multipoles 30-2500. That yields 82 full size bins and a partial last bin. Multipoles 2-29 are omitted to approach a Gaussian distribution, and to remove anomalies found in those first few multipoles, including a power deficit (*Planck* Collaboration 2014a). An additional simplification is the omission of polarization in the analysis. The approximate Gaussian distribution validates using the ln likelihood function, $\ln\mathcal{L}(p_1, p_2)$ (W. H. Press et al. 2007),

$$\ln\mathcal{L}(p_1, p_2) = \sum_{i=2}^{84} \frac{(\hat{\mathcal{D}}_i^{TT} - \mathcal{D}_i^{TT}(p_1, p_2))^2}{\hat{\sigma}_i^2} \quad (2)$$

where,

$$\mathcal{D}_i^{TT}(p_1, p_2) = \frac{\ell_i(\ell_i + 1)\mathcal{C}_i^{TT}(p_1, p_2)}{2\pi} \quad (3)$$

denotes an element of the binned computed temperature power-spectrum, entries $\hat{\mathcal{D}}_i^{TT}$ and $\hat{\sigma}_i^2$ represent the binned data points and corresponding variance, respectively, ℓ_i , the weighted multipole, and $\mathcal{C}_i^{TT}(p_1, p_2)$, the weighted multipole component, both within each bin, and p_1 and p_2 the two parameters that we choose to vary. We use the CLASS code to evaluate the temperature power spectra (D. Blas et al. 2016).

Six parameters determine the power spectrum configuration, h (as defined by the Hubble parameter, $H_0 = 100h \text{ km s}^{-1} \text{ Mpc}^{-1}$), $\Omega_b h^2$, the baryon fraction, $\Omega_c h^2$, the cold dark matter fraction, τ , the reionization optical depth, n_s , the spectral index, and A_s , the power spectrum amplitude. Since a precise evaluation of τ depends upon polarization data we adopt the value of 0.0543 found in *Planck* Collaboration (2020b), and use that value throughout. We will later find it convenient to substitute θ_s , the angular scale of the first acoustic peak, for h .

We initially choose h as one of the variables. The power spectrum amplitude factor, γ , serves as the second variable, and is consequential for rapid computation. Lensing has been incorporated in our investigation, which negates the linear relationship between A_s and the power spectra. Notwithstanding, for small excursions from the nominal amplitude, linearity is assumed with little error. That error is eliminated when Equation 1 is incorporated into the iterative process. A_s is set to a constant value within $\mathcal{D}_i^{TT}(h, A_s)$ and we as-

sume that $\mathcal{D}_i^{TT}(h, A_s) = \gamma y_i^{TT}(h)$, with all variation of A_s relegated to γ .

With that assumption, we take partial derivatives of Equation 2) and setting them to zero find,

$$0 = \sum_{i=2}^{84} \frac{(\hat{\mathcal{D}}_i^{TT} - \gamma y_i^{TT}(h))}{\hat{\sigma}_i^2} \gamma \partial y_i^{TT}(h) / \partial h \quad (4)$$

and,

$$0 = \sum_{i=2}^{84} \frac{(\hat{\mathcal{D}}_i^{TT} - \gamma y_i^{TT}(h))}{\hat{\sigma}_i^2} y_i^{TT}(h). \quad (5)$$

Figure 1a depicts the results attained using *Planck* parameter values (*Planck Collaboration 2020b*). The Hubble parameter is plotted along the abscissa, while the values of the partial derivatives of the ln likelihood are plotted along the ordinate.

The term, “pair” describes three different entities that are illustrated in Figure 1a. We compute two partial derivatives at a specific value along the abscissa, H_0 in this example. The resulting pair of points is labeled, 1, in the figure. When looking for which direction to continue the computation, we generate a pair of points, labeled, 2, in the figure. The direction to proceed to generate crossed lines for a particular value of γ is now evident. That is the first step towards a solution. A pair of crossed lines is our third use of the word. Each pair of the crossed lines is defined by a specific value of γ . Much like finding the root of a function with a single variable, once the zero line is bracketed by two pairs of crossed lines, we have the equivalent of the intermediate value theorem, and the solution on the zero line is readily found. The solution, with $\gamma = 1.00007$, $h=0.6785$ was derived by this bracketing and bisection technique. However, the dashed line in the figure shows that we can derive it directly from the crossed line pairs that straddle the zero line. The intersection of the dashed line with the zero line furnishes the value of H_0 , and interpolation provides the γ value of 1.00007. The value of h is higher than the value 0.6736 ± 0.0054 found in *Planck Collaboration (2020b)* but lies within 1σ of the result. Since we use only the TT spectra, an exact match is not expected. In Figure 1b we have expanded the distance between the line pairs, finding the same solution to four significant figures. In Section 3.3 a procedure is outlined to apply this technique in the general case to minimize the number of power spectra computation calls when neither parameter variable is linear.

3. ITERATIVE SOLUTIONS

3.1. Quasi-linear study

In Figure 1 we varied h , but any of the other parameters, i.e., $\Omega_b h^2$, $\Omega_c h^2$, and n_s can also be paired with A_s through $\mathcal{D}_i^{TT}(p, A_s) = \gamma y_i^{TT}(p)$. *A. Kosowsky et al. (2002)* introduced the use of the angular scale of the first acoustic peak, θ_s , as one of the parameters, and

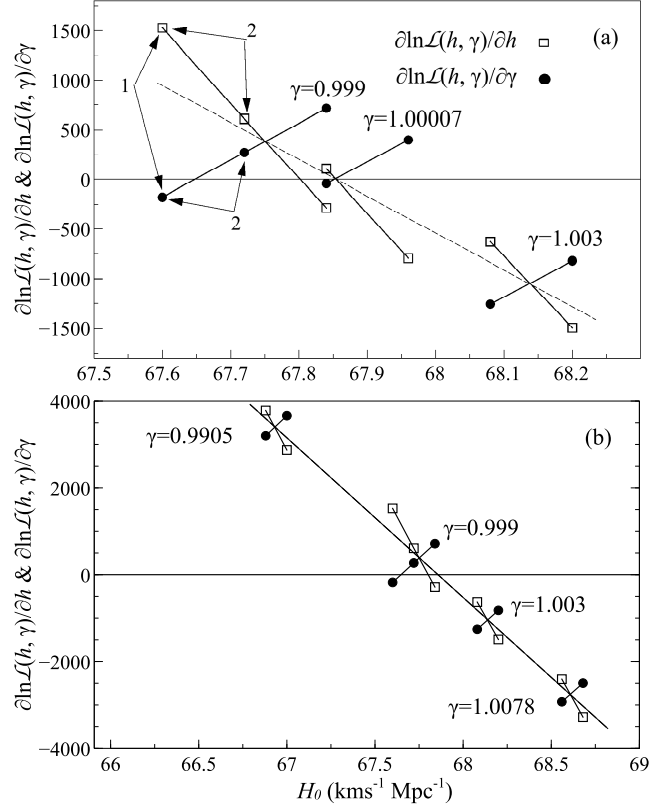


Figure 1. (a) Plots of $\partial \ln \mathcal{L}(h, \gamma) / \partial h$, and $\partial \ln \mathcal{L}(h, \gamma) / \partial \gamma$ versus H_0 for three pairs of crossed lines, each pair defined by a specific value of γ . The solution is found where a pair crossing lands exactly on the zero line, $\gamma=1.00007$, $h=0.6785$, in this instance. That is within 1σ of the *Planck* result. The dashed line demonstrates that the solution can be derived directly from two crossed line pairs that straddle the zero line. The fixed parameter values are (*Planck Collaboration 2020b*), $\Omega_b h^2=0.02237$, $\Omega_c h^2=0.1200$, $n_s=0.9649$, and $\tau=0.0543$. “Pair” of points such as those indicated with arrows and labeled, 1, are generated by the ln likelihood partial derivatives at specific values of H_0 . All points come in such pairs. “Pair” of points, such as those denoted with arrows and labeled, 2, are generated to determine line direction. (b) Expanded scale showing that crossed line pairs with larger separations than in (a) yield the same solution. Two crossed line pairs from (a) are shown to give a sense of scale.

subsequently that was adopted in CMB analysis as a substitute for h (*L. Verde et al. 2003*). We do the same here. The CLASS code angular scale, θ_s , is similar, but not identical to that defined by CAMB, θ_* .

Sequentially computing the 2D solution for each parameter, and substituting the latest value into $\mathcal{D}_i^{TT}(p, A_s) = \gamma y_i^{TT}(p)$ is an iterative process. We have conducted four iterative runs, each with a different set of initial parameter values. In two of the runs (one with 10 iterations to convergence, the other with 16)

Table 1. A sample from an iteration run that converged after 31 iterations. Shown are the initial parameter values, the results of the first two iterations, the result of the 15th iteration, and the results of the final two iterations. The entries for $10^9 A_s/\gamma$, such as the first one, 1.050275/1.78167, denote the value of A_s used in computing the parameter value immediately above, and the resulting value of γ derived from that computation. See text for further details.

	$100\theta_s$	$\Omega_b h^2$	$\Omega_c h^2$	n_s
	$10^9 A_s/\gamma$	$10^9 A_s/\gamma$	$10^9 A_s/\gamma$	$10^9 A_s/\gamma$
Initial values	—	0.03	0.1	1.2
Iteration #1	1.05190	0.01758	0.0708	1.1658
	1.050275/1.78167	1.871243/0.9935	1.859080/0.96855	1.800611/1.0141
Iteration #2	1.04372	0.02331	0.0649	1.1246
	1.826000/0.9866	1.801532/0.99417	1.791029/0.99323	1.778903/1.0174

Iteration #15	1.04225	0.02251	0.1160	0.9744
	2.074503/0.9998	2.074088/0.99995	2.073984/1.00165	2.077406/1.0012

Iteration #30	1.04180	0.02227	0.1203	0.9649
	2.101274/0.999995	2.101263/0.999995	2.101253/1.00004	2.101337/0.99997
Iteration #31	1.04180	0.02227	0.1203	0.9649
	2.101274/0.999995	2.101263/0.99999	2.101242/1.00003	2.101305/0.99998

we retain a fiducial value of $A_s = 2.100549 \times 10^{-9}$, and within specified ranges select the other parameter values at random. For the other two runs (19 and 31 iterations), we introduce the algorithm of Equation 1. That enables a choice to arbitrarily set an initial value for A_s . We additionally add a requirement that $\gamma \rightarrow 1$ at convergence. Table 1 provides a sample from one of those runs (31 iterations). The parameter, $100\theta_s$ is computed first, hence the lack of an initial value. The setting for the initial value for A_s was half that of our fiducial value (By contrast, the A_s initial value in the second run with the algorithm was twice the fiducial value. Initial values of the other parameters were likewise chosen to be dissimilar). The four runs yield the following results, $100\theta_s = 1.04179 \pm 0.000026$, $\Omega_b h^2 = 0.02227 \pm 0.000017$, $\Omega_c h^2 = 0.1205 \pm 0.00026$, $n_s = 0.9646 \pm 0.00057$, and $10^9 A_s = 2.102 \pm 0.0013$. We also extract values of H_0 from each run, and find, $H_0 = 67.6 \pm 0.1 \text{ km s}^{-1} \text{ Mpc}$. The variance between runs is tight. Despite our simplifications, all parameter values are in close agreement with the *Planck* results (*Planck Collaboration 2020b*).

We note the following specific; the computed values of γA_s in the two runs where A_s was kept at the fiducial value are in agreement with the computed values in the two runs where Equation 1 was employed. For the former pair, γ converges to a value exceeding unity by less than 0.1% for both runs. For the latter pair, γ converges to unity, but A_s converges to a value slightly greater than the fiducial value. In one run A_s is less than 0.1% higher than the fiducial value, in the other, about 0.15% higher.

The solution derivation examples given in Figure 1 show crossed lines that exhibit significant orthogonality. That follows too for the other parameters, with the exception of n_s . The crossed lines are close to parallel in that instance. The saving grace here is that the intersection of the crossed line pair with the zero line, is well defined. The uncertainty lies with the derived value of γ . Since γ is recomputed at each parameter step, any introduced error is immediately adjusted for in the following parameter step.

3.2. CMB parameter values as a function of ℓ_{max}

Much the same as for $\ell_{max}=2500$, we compute CMB parameter values for $\ell_{max}=959, 1019, 1139, 1199, 1259, 1379, 1439, 1499, 1769$, and 2009. (The binning of multipoles explains the seemingly odd choice for these values. Each represents the highest multipole of the last bin of the ℓ_{max} selection). The parameter values are presented in Table 2 along with the $\ell_{max}=2500$ results. At $\ell_{max}=1019$, in addition to the two modes obtained using *Planck* data, a single mode solution for *WMAP* is acquired. The variances are derived from the diagonal terms of the inverse Fisher information matrix. As the non-diagonal terms are all populated, that is an approximation that neglects correlations. The Fisher information matrix is formed by taking partial second derivatives of the \ln likelihood. That leads to sums of terms that include products of two partial derivatives, and second derivative terms multiplied by the differences of data and model multipole elements. That latter component is negligible, since the difference terms tend to cancel at the solution. Hence, numerical computation of the

Table 2. Compilation of CMB parameter values as a function of ℓ_{\max} . All values are computed using *Planck* data, with the exception of one point computed with *WMAP* data at $\ell_{\max}=1019$, and designated 1019W. The second column denotes the number of power spectrum peaks that lie within the range delineated by ℓ_{\max} . The peak numbers marked with a dagger, stipulate that those points lie at the summit of the indicated peak. A double dagger has been placed at $\ell_{\max}=1769$ to signify that it is one bin shy of the apex of the 6th peak, which lies at bin, $\ell_{\max}=1739$. $\ell_{\max}=1379$ is labeled 4/5 since although the apex of peak #5 has been removed, the remaining portion of that peak still affects parameter values. See text for discussion of mode B, found at those values of $\ell_{\max} \leq 1259$.

ℓ_{Max}	#peaks	$100\theta_s$	$\Omega_b h^2$	$\Omega_c h^2$	n_s	$10^9 A_s$	h 0.1ln likelihood
959	3	1.04082±0.00072	0.02222±0.00031	0.1184±0.0028	0.9650±0.0097	2.089±0.013	0.680±0.0024 2.1806
959B	3	1.04103±0.0014	0.02232±0.00064	0.1175±0.0028	0.9682±0.01	2.085±0.013	0.684±0.0047 2.1848
1019	3	1.04083±0.00069	0.02221±0.00031	0.1185±0.0028	0.9651±0.0098	2.089±0.012	0.679±0.0023 2.1927
1019B	3	1.04105±0.00070	0.02234±0.00031	0.1173±0.0027	0.9693±0.0099	2.084±0.012	0.685±0.0024 2.2049
1019W	3	1.04109±0.0018	0.02238±0.00042	0.1156±0.0041	0.9648±0.011	2.070±0.029	0.692±0.0062
1139	4†	1.04124±0.00048	0.02237±0.00023	0.1172±0.0020	0.9701±0.0063	2.084±0.010	0.687±0.0016 2.5839
1139B	4†	1.04125±0.00048	0.02240±0.00023	0.1170±0.0020	0.9707±0.0063	2.083±0.010	0.688±0.0016 2.5845
1199	4	1.04119±0.00048	0.02230±0.00022	0.1178±0.0019	0.9679±0.0054	2.087±0.0095	0.684±0.0016 2.6215
1199B	4	1.04123±0.00048	0.02234±0.00021	0.1174±0.0018	0.9690±0.0054	2.085±0.0095	0.686±0.0016 2.6094
1259	4	1.04139±0.00046	0.02221±0.00021	0.1187±0.0018	0.9645±0.0053	2.091±0.0095	0.680±0.0015 3.3284
1259B	4	1.04144±0.00045	0.02224±0.00021	0.1184±0.0018	0.9653±0.0053	2.090±0.0096	0.682±0.0015 3.3358
1379	4/5	1.04203±0.00041	0.02244±0.00020	0.1187±0.0018	0.9688±0.0052	2.094±0.0092	0.684±0.0014
1439	5†	1.04195±0.00038	0.02235±0.00018	0.1193±0.0017	0.9666±0.0046	2.097±0.0089	0.681±0.0013
1499	5	1.04194±0.00038	0.02220±0.00016	0.1200±0.0017	0.9636±0.0043	2.100±0.0088	0.677±0.0011
1769	6††	1.04174±0.00033	0.02221±0.00014	0.1205±0.0016	0.9637±0.0039	2.102±0.0083	0.675±0.0011
2009	7†	1.04176±0.00032	0.02228±0.00014	0.1205±0.0015	0.9646±0.0037	2.102±0.008	0.676±0.0013
2500	8	1.04179±0.00032	0.02227±0.00013	0.1205±0.0015	0.9646±0.0037	2.102±0.008	0.676±0.0011

second derivatives is not necessary (W. H. Press et al. 2007).

Table 2 also lists the number of power spectrum peaks within the multipole range defined by each ℓ_{\max} . Any change in parameter values as we decrease ℓ_{\max} must be ascribed to a loss of information carried by the culled multipoles. H_0 is plotted as a function of ℓ_{\max} in Figure 2, and we use that figure to describe the results, starting at the high end, $\ell_{\max}=2500$. That range encompasses eight power spectrum peaks. Peak #1 is nearly fifty times greater than peak #8, and about twenty-five greater than peak #7, and there is virtually no change

in parameter values when peaks #8 and #7 are eliminated. With the removal of peak #6 there is a small, but noticeable change in H_0 at $\ell_{\max}=1499$, and that change becomes more pronounced as we cut into peak #5.

At $\ell_{\max}=1259$ the effect of stripping away multipoles is substantial. The loss of peak #5 has impacted the computed parameter values such that there is now a major transformation. Enough uncertainty in the solution has been introduced to support a second mode, which we refer to as mode B. For $\ell_{\max}=1199$, and 1139 the situation is similar to that of $\ell_{\max}=1259$, although

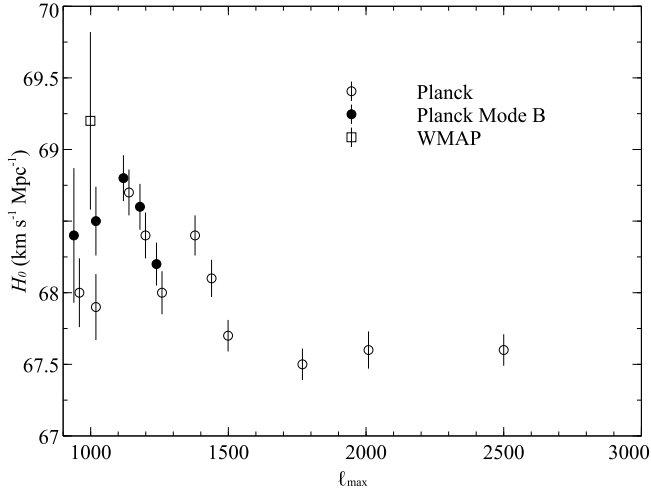


Figure 2. Plot of H_0 versus ℓ_{\max} . For those values of ℓ_{\max} that confine no more than three, or four power spectrum peaks, i.e., 959, 1019, 1139, 1199, and 1259, a bimodal solution is obtained. With the exception of 1019B, all B mode points, and, additionally, the 1019(WMAP) point are shifted to the left for clarity.

$\ell_{\max}=1139$ and 1139B lie at the apex of peak #4, and the computed H_0 values reach a maximum at that point. At the ℓ_{\max} values of 1019 and 959 only the first three peaks remain, and the spread between the two modes has increased markedly. The designation “parameter value” is something of a misnomer for all values of $\ell_{\max} \leq 1259$, the bimodal solution being a non-physical condition.

Turning to Table 2, we address a couple of specifics. First, the variances at $\ell_{\max}=2500$ are in agreement with the values obtained by the *Planck* Collaboration (*Planck* Collaboration 2020b), with the major exception of our H_0 variance, which is significantly lower than that derived by *Planck*. After attaining convergence, and computing the variances with θ_s as one of the parameters, we then solve for h , substitute that value of h for θ_s in the CLASS program, verify that it yields the same power spectrum, and finally, recompute the variances with h , rather than with θ_s . In addition to finding the variance for h , the other variances (except for that of θ_s) are recomputed along with it, with no change in their values. That procedure instills confidence that our derived values of h variances are valid. The second particular with respect to Table 2 is the inclusion of the \ln likelihood value for each mode for all ℓ_{\max} values that exhibit a bimodal solution. The MLE translates to a minimum in the \ln likelihood (for convenience a minus sign has been removed from our definition of \ln likelihood), and the global maximum is the lower of the two values. For four of the points the base mode is at the global maximum. However, for $\ell_{\max}=1199$, mode B is

at the global maximum, and we are not able to reach a general conclusion.

Where we can generalize, is with respect to the different paths to convergence taken by the two modes. In the iterative process to obtain a solution, mode B manifests a distinct difference from the base mode in that it has a “flat” behavior as convergence is approached. What we mean by “flat” is that even when the various parameters, $100\theta_s$, $\Omega_b h^2$, $\Omega_c h^2$, n_s , and $10^9 A_s$ are within a digit or two of the solution in their last significant place, several more iterations are required to reach convergence. Strictly speaking convergence was never obtained for the $\ell_{\max}=1139$, and 1199 mode B solutions. An acutely narrow set of parameter values wandered, but never found a “bottom”.

We are now in a position to address the variety of CMB H_0 results. The discrepancy between CMB derived results and low red shift results falls outside of our scope of work. However, we note that a recent paper (M. Kamionkowski & A. G. Riess 2023), reviews models, specifically early dark energy (EDE) models, that possibly explain the disparity between low red shift and CMB measurements. Further refinement of CMB data is necessary before any conclusions can be reached.

There are two CMB results that require an explanation, that of *WMAP*, with $\ell_{\max}=1200$, $H_0=70.0 \pm 2.2$ km s⁻¹ Mpc⁻¹ (G. Hinshaw et al. 2013), and secondly that of G. E. Addison et al. (2016) using *Planck* data with $\ell_{\max}=1000$, 69.7 ± 1.7 km s⁻¹ Mpc⁻¹. The *WMAP* and *Planck* power spectra are in excellent agreement in this multipole range (see *Planck* Collaboration (2016), figure 48), except for the error level, which is significantly higher for *WMAP*. That in and of itself can explain why though our computation with the *Planck* data yields two modes, that with the *WMAP* data yields one. The difference between the two closely spaced modes is obscured in the *WMAP* computation due to the higher values of σ . Regarding the analysis in G. Hinshaw et al. (2013) and G. E. Addison et al. (2016), there are two points to be made. First, both studies employed MCMC to evaluate the parameters. MCMC is deficient when evaluating multimodal solutions, and in particular when only a single mode is anticipated. Second, both results have large variances, and our computations of H_0 in the relevant range $\ell_{\max}=959$ to 1259 fall well within a standard deviation of either result.

The main conclusion we take away concerning the dependence of CMB parameters on ℓ_{\max} , is that to arrive at an accurate solution, the spectrum should include six or more peaks. Spectra with fewer than six peaks may serve some purpose for diagnostics, but not for computing useful parameter values.

3.3. General Case

In the general case, one of the \ln likelihood partials can no longer be generated by simple multiplication, and the required number of power spectra calls, or an analo-

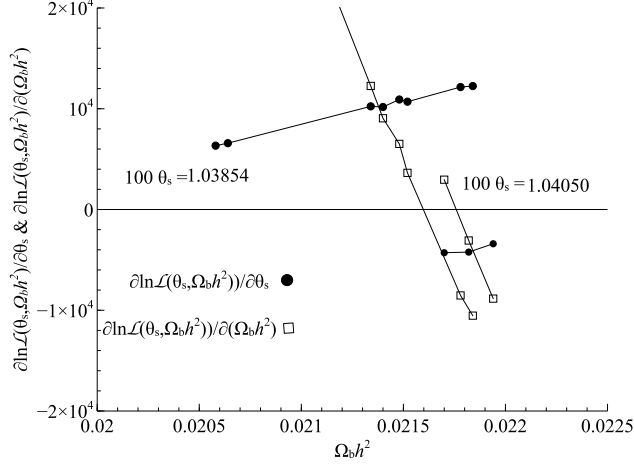


Figure 3. Plots of $\partial \ln \mathcal{L}(\theta_s, \Omega_b h^2) / \partial (\Omega_b h^2)$, and $\partial \ln \mathcal{L}(\theta_s, \Omega_b h^2) / \partial \theta_s$ versus $\Omega_b h^2$ for two pairs of crossed lines. All points for both crossed line pairs require calls for power spectra computation for both components of the ln likelihood partial derivatives. The crossed line pairs straddle the zero line, and the intercept connecting the cross point of each line pair, and interpolation, provide an approximate solution, $\Omega_b h^2 = 0.02171$, and $\theta_s = 1.03994$. The connecting line is omitted in the figure for clarity. The actual solution is $\Omega_b h^2 = 0.02172$, and $\theta_s = 1.04000$. Several pairs of points are plotted to demonstrate how the line crossings were located. As depicted in Figure 1a, the ln likelihood partial derivatives generate a pair of points for each specific parameter value along the abscissa. The seeming lack of these pairs at the left is a result of the complimentary points falling beyond the figure limits.

gous entity for a non-CMB application, is substantially increased. Maintaining the focus on CMB, the metric by which we judge the effectiveness of a computational method is the number of calls to generate power spectra. For the example illustrated in Table 1 fewer than 600 calls were required. The other three runs each required 400 or fewer calls. To tally the number of power spectra calls we must account for numerical computation of the partial derivatives. Symmetric numerical differentiation is implemented to evaluate those partial derivatives. For our quasi-linear approach, an isolated point requires three power spectra calls. Generally, within a neighborhood, equally spaced points are effected to minimize the number of calls used exclusively to compute derivatives. As demonstrated in Figure 1a, when searching for the crossing of two lines, we routinely create a pair of points to determine which direction to proceed. That necessitates four power spectra calls in the quasi-linear case. Figure 3 depicts a two parameter example in which $100\theta_s$, and $\Omega_b h^2$ are the two variables, and we no longer have a quasi-linear condition. The pairs of points in that figure require eight power spectra calls

for each pair, as derivatives must be generated for both components of the partials.

As shown in Figure 1, once the zero line is straddled by two pairs of crossed lines, the intercept of the line connecting the cross-points of each pair with the zero line identifies one parameter value to a good approximation, and interpolation identifies the other. This procedure provides a means of reducing the number of power spectra calls. A prudent tactic is to implement the technique, and use it to generate a value at the indicated point, putting it to the test, and rapidly closing in on a solution. This interception and interpolation technique is one of three mitigating factors with regard to the required number of power spectra calls in the general case. The second mitigating factor concerns the migration of parameter values to the vicinity of their final states well before final convergence. Thus, in the example of Table 1, all iterations after the fifth required less than 20 calls, that is 4-6 calls per parameter step. Hence, in the general case, even if the number of calls per parameter step should increase quadratically in comparison with the quasi-linear condition, that number is still within reasonable bounds. The third moderating factor pertains to evaluating two parameters together. In our quasi-linear example four steps were required for one iteration. Taking two variables at once, as in Figure 3, would require three steps per iteration, and in applications with larger numbers of parameters, the number of steps needed reduces to close to half those required in the case of a linear parameter paired one at a time with the others.

4. DISCUSSION

Within the context of multi-parameter likelihoods, two-dimensional analysis is a relatively simple procedure, made more so by the ability to visualize and plot solutions. Making use of that facility entails setting all parameters, other than two, to fixed values and solving for those two parameters. The full potential of that approach is realized when iteration is introduced. All parameters are cyclically evaluated, and convergence to a solution follows.

The key to regulation of computation time is the number of calls for computation of the appraised function. For the general case, when neither variable is linear with respect to the function, calls are made over a two-dimensional grid, and the number of calls can become unwieldy. We have identified two techniques, one regarding interpolation, the other evaluating two different parameters at each step, that reduce the number of calls, and we have also noted that the number of calls decreases sharply with increasing iteration count. These factors keep the number of calls manageable. However, no technique can outperform the great reduction in calls that occurs when one of the variables approaches linearity. That is the situation with the lensed CMB power spectrum, and the result is that we are able to evalu-

ate the cosmological parameters in good agreement with *Planck*, while calling for power spectra no more than several hundred times. That gives this 2D iterative method a decided edge over MCMC for the same computation. For the general case, when neither variable is linear, we estimate thousands of calls per run. We posit that in the general case, the 2D iterative method still compares favorably with MCMC computation.

In our extended example of deriving cosmological parameters from power spectra we evaluate the cosmological parameters as a function of ℓ_{\max} . The first three peaks of the CMB power spectra contain a large amount of information, and many cosmological details can be extracted from their positions and relative heights (W. Hu et al. 2001). Our emphasis is on how the parameter values change as multipoles are stripped from the spectra. In that context we conclude that at least six power spectrum peaks are required to provide accurate parameter values. Further, when the number of peaks is reduced to four, enough information has been

jettisoned to lead to a bimodal solution. That bimodal solution was not detected by *WMAP*, and the higher value of H_0 found at low values of ℓ_{\max} contributed to a delay in comprehending that the CMB derived value of H_0 was incompatible with that derived from low red shift measurements. It was a short delay, as the *Planck* evaluation at $\ell_{\max}=2500$ followed right on the heels of the *WMAP* assessment.

Though this study draws upon examples from cosmology, the 2D iterative method could find application in many areas where MCMC calculations are required to evaluate multi-parameter functions.

ACKNOWLEDGMENTS

We acknowledge the use of the Legacy Archive for Microwave Background Data Analysis (LAMBDA), part of the High Energy Astrophysics Science Archive Center (HEASARC). HEASARC/LAMBDA is a service of the Astrophysics Science Division at the NASA Goddard Space Flight Center.

REFERENCES

- Addison, G. E., Huang, Y., Watts, D. J., et al., *ApJ*, 818, 132 (2016)
- Aiola, S., Calabrese, E., Maurin, L., et al., *JCAP*, 12, 047 (2020)
- Balkenhol, L., Dutcher, D., Mancini, A. Spurio, et al., *PhRvD* 108, 023510 (2023)
- Blas, D., Lesgoues, J., & Tram, T., *JCAP*, 7, 034 (2011)
- Choi, S.K., Hasselfield, M., Ho, S.-P., et al., *JCAP*, 12, 045 (2020)
- Freedman, W.L., Madore, B.F., Hatt, D., et al., *ApJ*, 882, 34 (2019)
- Hastings, W.K., *Biometrika*, 57, 97 (1970)
- Hinshaw, G., Komatsu, E., Spergel, D.N., et al., *ApJS*, 208, 19 (2013)
- Hu, W., Fukugita, M., Zaldarriaga, M., & Tegmark, M., *ApJ*, 549, 669 (2001)
- Kamionkowski, M., Riess, A.G., *ARNPS*, 73, 153 (2023)
- Kosowsky, A., Milosavljevic, M., & Jimenez, R., *PhRvD* 66, 063007 (2002)
- Metropolis, N., Rosenbluth, A.W., Rosenbluth, M.N., et al., *JChPh*, 21, 1087 (1953)
- Percival, W. J. & Brown, M. L., *MNRAS*, 372, 1104 (2006)
- Planck* Collaboration, *A&A* 571, A1 (2014a)
- Planck* Collaboration, *A&A*, 571, A16 (2014b)
- Planck* Collaboration, *A&A*, 594, A11 (2016)
- Planck* Collaboration, *A&A*, 641, A5 (2020a)
- Planck* Collaboration, *A&A*, 641, A6 (2020b)
- Press, W.H., Teukolsky, S.A., Vetterling, W.T., & Flannery, B.P. 2007, *Numerical Recipes*, (3rd ed.; New York, NY: Cambridge Univ. Press)
- Riess, A.G., Yuan, W., Macri, L.M., et al., *ApJL*, 934, L7 (2022)
- Verde, L., Peiris, H. V., Spergel, D. N., et al., *ApJS*, 148, 195 (2003)
- Verde, L., Schöneberg, N., & Gil-Marín, H., *ARA&A*, 62, 287 (2024)